Journal of Geodesy (2025) 99:77
https://doi.org/10.1007/s00190-025-02002-z

ORIGINAL ARTICLE

Bridging missing GNSS phase measurements through cycle slip detection for improved smartphone positioning

Jiahuan Hu[1] · Wu Chen[1] · Pan Li[2] · Xiaolong Mi[1] · Kai Zheng[3] · Long Tang[4] · Wanke Liu[5] · Jingkai Yuan[2] · Sunil Bisnath[6]

Received: 1 May 2025 / Accepted: 3 September 2025 / Published online: 21 September 2025

Abstract

Smartphone-related location-based services (LBSs) are among the most frequently used applications in daily life. The accuracy of smartphone global navigation satellite system (GNSS) positioning is limited to approximately ten-meter to meter-level precision due to poor observation quality and obstructed environments. For smartphone GNSS data, the phase measurements are frequently missing, which are treated as cycle slips in traditional algorithms, leading to the reset of ambiguity and variance, thereby decreasing positioning performance. To address this issue, this study proposes bridging the phase data gap in smartphone precise point positioning by utilizing previously available measurements before the signal outage to perform cycle slip detection, aiming to avoid excessive parameter resets in the filter. Indicators, including test values of geometry-free (GF) combination, code-minus-phase (CMP) combination, differences between Doppler and time-differenced carrier phase (TDCP), and pre-fit phase residuals, are selected to determine whether to reset the ambiguity and variance for a missing phase measurement. The proposed method is validated with 10 smartphone datasets collected in driving environments. The percentage of positioning errors within 1.5 m is improved from 65.1 to 99.1% for one of the Samsung S21 + phones. For a Mi 8 phone, the 68th and 95th percentile positioning errors are improved by ~ 2 dm. The overall statistics of the ten datasets demonstrate the correctness and efficiency of the proposed method, showing improvements in positioning errors within 1.5 m and 1 m by 4.3% and 8.2%, respectively. Moreover, the potential application of the proposed algorithm is validated with a geodetic dataset, showing significant positioning accuracy improvement when the signal outage occurs.

Keywords Cycle slip · Measurement bridging · Precise point positioning · Phase data gap · Smartphone positioning

1 Introduction

Global navigation satellite system (GNSS) can provide ten-meter-level to millimeter-level positioning performance depending on the grade of receivers and processing modes (Zangenehnejad and Gao 2021; Wang et al. 2024; Huang et al. 2023; Shu et al. 2025). In mass-market applications, smartphones are among the most frequently used sensors for delivering location-based services to vehicles and pedestrians, owing to their convenient, low-cost, and ubiquitous properties (Bisnath and Aggrey 2024; Fu et al. 2020). However, the positioning accuracy of smartphones typically ranges from ten-meter-level to meter-level, primarily due to the noisy and limited measurements caused by the linearly polarized embedded antennas and signal-obstructed realistic environments (Realini et al. 2017; Laurichesse et al. 2017; Wang et al. 2021).

✉ Pan Li
lipan@chd.edu.cn

1 Department of Land Surveying and Geo-Informatics, The Hong Kong Polytechnic University, Hong Kong, China

2 College of Geology Engineering and Geomatics, Chang'an University, Xi'an, China

3 School of Navigation, Wuhan University of Technology, Wuhan, China

4 School of Civil and Transportation Engineering, Guangdong University of Technology, Guangzhou, China

5 School of Geodesy and Geomatics, Wuhan University, Wuhan, China

6 Department of Earth and Space Science and Engineering, York University, Toronto, ON M3J 1P3, Canada

With raw GNSS measurements accessible from Android smartphones (Malkos 2016), research has been conducted to improve smartphone positioning accuracy in various aspects, including raw measurement quality assessment (Paziewski et al. 2019), positioning performance evaluation with different positioning methods (Li et al. 2022a), stochastic modeling (Hu et al. 2024), smartphone-specific quality control method, and ambiguity resolution (Zhang et al. 2024; Jiang et al. 2023). The existing research shows that the pseudorange noise of smartphones can reach tens of meters in urban canyon environments (Liu et al. 2019), resulting in ten-meter-level standard point positioning (SPP) accuracy with code measurements (Sikirica et al. 2017; Paziewski et al. 2020). Moreover, the measurement quality from different frequencies and constellations exhibits slight differences, e.g., code measurements from GLONASS were reported to be noisier than those from other constellations, and meanwhile, measurements on GPS L5 and Galileo E5a are more precise than those on L1 and E1 (Robustelli et al. 2019; Hu et al. 2023).

The use of carrier-phase measurements enables more accurate positioning performance with real-time kinematic (RTK) and precise point positioning (PPP) (Miao et al. 2022; Tao et al. 2023). However, it also brings difficulty in handling the ambiguity parameters in phase observations. Cycle slips, which could be caused by very-low signal–to–noise ratio (SNR), failure of the receiver software, or malfunctioning satellite oscillator, represent a significant obstacle to fully leveraging the precise phase measurements (Langley et al. 2017). A detected cycle slip indicates phase measurement discontinuity and a jumped cycle-count ambiguity. In filtered solutions, the ambiguities, which are theoretically integers, are estimated as float constants because of the effect of multipath and unmodeled errors. The ambiguity parameter and variance gradually converge in the filter during a continuous phase arc. However, once there is a signal outage or phase cycle slip occurrence, the corresponding ambiguities and their variance will be reset and reconverge (Everett et al. 2022). Such strategy performs well with geodetic receivers, where signal loss or cycle slips are infrequent. Conversely, frequent phase measurement loss is noticed in smartphone GNSS data. The phase data gaps lead to frequent resets and reconvergences of ambiguities, thereby affecting the stability and accuracy of positioning solutions. For instance, an intuitive and sharp contrast can be seen: Filtered solutions are smoother than single-epoch (the parameters are reset every epoch) solutions.

To accommodate satellite signals with available code measurements but missing corresponding phase observations, Yi et al. (2024) evaluated the code noise of these measurements and incorporated them into PPP processing, demonstrating positioning performance improvements. However, the frequent reset issue raised by the phase data gaps has not been adequately addressed or resolved. Therefore, this study seeks to bridge the phase data gaps from the perspective of cycle slip detection, aiming to minimize excessive ambiguity and variance resets and to provide stable and accurate PPP performance with smartphones. The main novelty and contributions are as follows:

(1) Different from the existing research in which the phase data gaps are universally treated as cycle slips, this study proposes bridging the phase data gaps through detecting cycle slips using measurements before and after the signal outage. This approach significantly reduces the frequency of ambiguity and variance resets in data processing.
(2) Given that the conventional Doppler cycle slip detection method is not applicable in smartphones due to inconsistent phase clocks, an improved satellite-differenced Doppler cycle slip detection method is introduced to eliminate the clock datums.
(3) Satellite measurement databases and four checks are designed to bridge the phase data gaps. These include the phase pre-fit residual check, as well as three cycle slip test values. The efficacy of the proposed algorithm is validated using ten datasets collected in realistic driving environments. Moreover, the potential application of the proposed algorithm is validated with a geodetic dataset.

The mathematical model of smartphone PPP, along with the proposed phase gap bridging method, is introduced first. The assessment of measurement availability and the efficiency validation of the improved Doppler cycle slip detection method are conducted, followed by the positioning performance evaluation. Finally, conclusion and future work are provided.

2 Method

Most GNSS chips in smartphones (e.g., Samsung S21+) support collecting dual-frequency measurements for GPS (L1/L5) and Galileo (E1/E5a), and single-frequency observations for BDS (B1) and GLONASS (L1). Several modern smartphones can also track QZSS L1/L5 and BDS multi-frequency measurements (e.g., Xiaomi Mi8, Redmi K50 and Huawei Mate 40). The raw pseudorange (P) and carrier-phase (L) measurements derived from Android devices can be formulized as:

$$\begin{cases} P_j^s = \tilde{\rho}^s + c(dt_r + isb^{sys} - dt^s) + \gamma_j I_1^s + T^s + b_{j,r}^s + \varepsilon_j^s \\ L_j^s = \tilde{\rho}^s + c(dt_r + isb^{sys} - dt^s) - \gamma_j I_1^s + T^s + \lambda_j (N_j^s + B_{j,r}^s) + \xi_j^s \end{cases} \tag{1}$$

where the raw measurements are in units of meters. s and j are the satellite and frequency notations, respectively. ρ is

satellite-receiver geometric range corrected by existing error models such as satellite phase center offset and variation, relativistic effect, phase windup, and satellite differential code bias (Kouba 2009). c is the speed of light, and dt_r is the receiver clock offset to be estimated, while dt^s is the satellite clock offset and is corrected using products from analysis centers. For multi-GNSS data processing, inter-system clock bias is introduced, as denoted by isb^{sys}. For GPS, the inter-system bias is zero, while the constellation-related bias term is estimated for other constellations. I_1^s is the slant ionospheric effect on the first frequency and is estimated in the filter, while the ionospheric effect of other frequencies can be calculated by multiplying the coefficient γ_j, with $\gamma_j = (f_1/f_j)^2$. T^s refers to the slant tropospheric delay and can be divided into wet and hydrostatic components. The hydrostatic part can be corrected with empirical model, while the wet component is estimated as a function of wet mapping (MF) function and zenith wet delay (ZWD). λ_j is the wavelength, and N_j^s is the integer ambiguity. $b_{j,r}^s$ and $B_{j,r}^s$ are code and phase hardware biases, respectively. ε_j^s and ξ_j^s are code and phase observation noise and multipath. Moreover, the conventional carrier–to–noise (C/N_0)-based weighting scheme is adopted in this study as

$$\sigma_{C/N_0}^2 = a_{C/N_0}^2 + b_{C/N_0}^2 * 10^{\frac{-0.5*snr}{10}} \tag{2}$$

where σ_{C/N_0}^2 is calculated weighting variances. a_{C/N_0}^2 and b_{C/N_0}^2 are the unit-weight mean-square errors. snr is SNR value from receiver independent exchange (RINEX) format observation file. The coefficients used in this study can be found in Table 1, which are fitted using range errors from different constellations and frequencies, and are used as empirical values (Hu et al. 2024). The code precision can be calculated using Eq. (2), while the precision of phase measurements is 1/100 of the corresponding code measurements.

The extended Kalman filter (EKF) is normally employed to estimate unknown parameters in smartphone precise point positioning, in which the state vector and variance–covariance matrix predictions are of vital importance, as they provide a priori information for the subsequent epoch. The transition matrix for ambiguity parameters is generally set as an identity matrix, as they are constant if no cycle slip or signal blockage occurs. Currently, four commonly used cycle slip detection methods, applicable to either single- or dual-frequency measurements, are adopted in smartphone GNSS data processing. These include the Melbourne–Wübbena (MW) combination, the geometry-free (GF) combination (Blewitt 1990), the code-minus-phase (CMP) method, and Doppler cycle slip detection method. The latter compares the difference between Doppler measurement and time-differenced carrier phase (TDCP) (Li et al. 2022b) and is abbreviated as DTDCP method in the following sections. The test values of these methods are:

$$\begin{aligned}\nabla MW_{15}^s &= MW_{15}^s(t) - MW_{15}^s(t-1) \\ &= \nabla\left(\frac{f_1 L_1^s - f_5 L_5^s}{(f_1 - f_5)} - \frac{f_1 P_1^s + f_5 P_5^s}{f_1 + f_5}\right)\end{aligned} \tag{3}$$

$$\nabla GF_{15}^s = GF_{15}^s(t) - GF_{15}^s(t-1) = \nabla(L_1^s - L_5^s) \tag{4}$$

$$\nabla CMP_j^s = CMP_j^s(t) - CMP_j^s(t-1) = \nabla(P_j^s - L_j^s) \tag{5}$$

$$\nabla DTDCP_j^s = \frac{\nabla L_j^s}{\lambda_j} + \frac{(D_j^s(t) + D_j^s(t-1))}{2} \cdot \Delta t \tag{6}$$

where ∇ is time-differencing operator, D denotes Doppler measurement, and Δt is the time interval between epochs t and $t-1$. When the calculated test values exceed the given thresholds, or if there is a signal outage for a specific phase measurement, the ambiguity and its variance will be reset in the EKF, resulting in a re-convergence for the ambiguity parameter.

In realistic smartphone GNSS measurements, the phase measurements are frequently missing, resulting in numerous variance resets and decreased positioning performance. However, whether cycle slips truly occur during signal outages is worth investigating. This study tries to bridge the missing phase measurements by detecting cycle slips using measurements before and after the phase missing. Specifically, the period during which the phase measurements are unavailable can be considered as having a longer sampling interval. For instance, if the original data interval is 1 s, and only phase measurements for satellite G01 are missing for ten epochs (10 s), whether resetting the variance of ambiguity for G01 in the filter can be decided by detecting cycle slips using the current measurements and those taken 10 epochs earlier. In this case, the interval for G01 is regarded as 10 s, whereas it is still 1 s for satellites with continuous phase measurements, as

$$\Delta t = \begin{cases} 10 \text{ s, sat = G01} \\ 1 \text{ s, sat = others} \end{cases} \tag{7}$$

Therefore, the key to bridging the phase measurement gaps lies in properly detecting cycle slips over longer time intervals. It is important to ensure that the bridged phase measurements are free of cycle slips, as any undetected cycle slip would degrade positioning performance if the corresponding filter variance is not reset. Consequently, CMP method is employed only as a supplementary of the GF and DTDCP methods, given that the MW and CMP measurements are significantly affected by pseudorange noise.

Although the GF and DTDCP methods can be applied in detecting smartphone cycle slips, each has its limitations.

Table 1 Constellation and frequency-specific weighting function coefficients

Band	a_{C/N_0}	b_{C/N_0}	Band	a_{C/N_0}	b_{C/N_0}
GPS L1	2.86	243.37	GAL L1	3.77	160.89
GPS L5	2.11	56.82	GAL L5	1.74	59.77
GLO L1	10.17	288.12	BDS L1	4.64	194.30

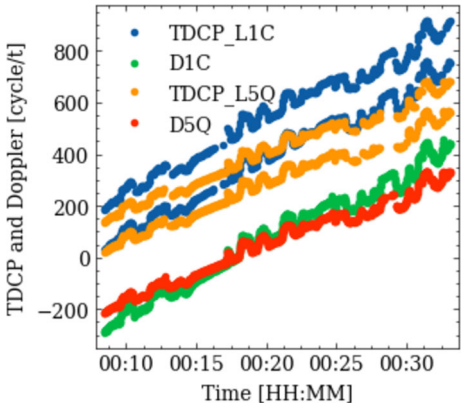

Fig. 1 Time series of TDCP and Doppler measurements on L1 and L5 for satellite E21 collected with a Samsung S21 + phone on August 20, 2021

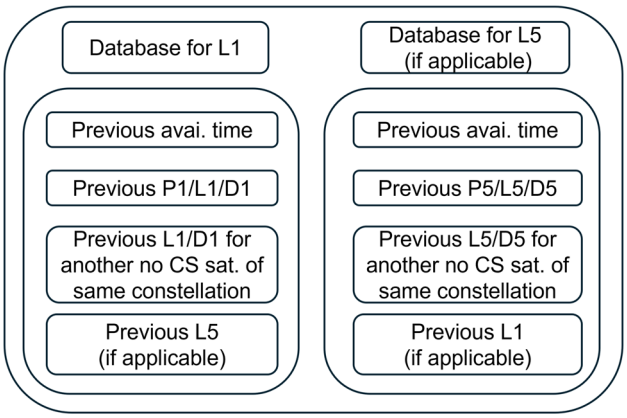

Fig. 2 Simplified satellite database used in bridging the phase gaps. Previously available timestamps and measurements were stored for L1 and L5 of each satellite

GF method relies on dual-frequency measurements and cannot detect cycle slips when their ratios are close to or equal to the ratio of the wavelengths of the two frequencies. In comparison, DTDCP method is sensitive to small cycle slips and is applicable in single-frequency measurements. However, it is found that for some smartphones (e.g., Xiaomi Mi8 and Samsung S21+), the TDCP measurements fluctuate because of frequent receiver clock jumps. Additionally, TDCPs and Doppler measurements for the same satellite are not consistent, causing challenges in bridging data gaps with the DTDCP method (Zangenehnejad et al. 2022). Figure 1 provides an example for the mentioned issue, in which the TDCP and Doppler measurements of satellite E21 from a Samsung S21 + phone are illustrated. It is clear that there are two distinct segments (e.g., two blue and two orange lines) for TDCP measurements, and significant differences between TDCP and Doppler are noticed. The two TDCP curves are temporally aligned, which is similar to the results in Zangenehnejad et al. (2022), and the possible reason might be the embedded time synchronization procedure within the smartphones. The two segments are caused by frequent phase clock jumps. Moreover, the reason why they appear to look like two lines is that the dots are used in the plotting instead of lines, because the lines will result in one big wide line, which would make the results appear ambiguous.

To deal with this issue, Hu et al. (2024) propose to set a datum for the DTDCP test values, i.e., the DTDCP test values can be regarded as a generalized normal distributed mean-shift model, as Eq. (8), in which the constellation and frequency-specific datum are calculated for every epoch, and Γ_{DTDCP} is the noise level of Eq. (6) calculated with error propagation law.

$$(DTDCP^{s}_{j,t} - datum_{j,t}) \sim N(0, \Gamma_{DTDCP}) \tag{8}$$

Despite the modified DTDCP method performing well for a unified time interval, challenges arise when the time intervals are larger and vary across different satellites. These variations lead to changes in the datums, making Eq. (8) inapplicable. For instance, if phase measurements for satellite G01 are missing for 10 epochs, the calculated DTDCP test value for G01 may significantly differ from those of other satellites with normal measurements. This discrepancy occurs because the datums change every epoch and are difficult to predict. To deal with this issue, a method is proposed in this study to transfer the previously available datum to the current epoch. This is achieved by forming between-satellite-differenced DTDCP measurements for the two epochs, using reference measurements on the same frequency from satellite n within the same constellation, as

$$\nabla DTDCP^{sn}_{j} = (DTDCP^{sn}_{j})_{t} - (DTDCP^{sn}_{j})_{t-1} \tag{9}$$

A simplified satellite measurement database, designed for bridging the phase gaps, is presented in Fig. 2. For each satellite, information about the epoch where the previous phase measurement is available is stored. The databases for L1 and

L5 are organized separately, i.e., the epochs of previously available phase measurements on L1 and L5 may differ. The previously available timestamp is utilized to calculate the updated interval, and the corresponding code, phase, and Doppler measurements are stored as well. Moreover, the phase and Doppler measurements from another no-CS satellite within the same constellation are included. If applicable, the phase measurement on the other frequency is also saved. It is worth noting that, in the collected smartphone data, the pseudorange and Doppler measurements are always recorded when there is an available phase measurement. Therefore, the proposed algorithm is not affected by the case when code or Doppler measurements are missing.

With the stored databases, the proposed algorithm is implemented as follows, aiming to ensure that the bridged ambiguities are free of undetected cycle slips to the greatest extent possible. Moreover, to accommodate possible unmodeled errors and atmospheric residuals absorbed in float ambiguities, when all the following conditions are met, the float ambiguity values are kept, while the corresponding ambiguity variances in EKF are increased to twice the previously available variance information.

(1) CMP combination check. The time-differenced CMP measurements contain ionospheric residuals, hardware biases, and the ambiguity changes. For smartphone data with an interval of 1 s, the ionospheric residuals can be disregarded. Considering the noise level of code measurements, once the epoch-differenced CMP exceeds 2 m, the corresponding ambiguity and its variance are reset.
(2) GF combination check. Time-differenced GF measurements are applied to detect possibly cycle slips for dual-frequency measurements. Only if the value is below a given threshold (0.05 m in this study), the phase measurement is bridged.
(3) DTDCP check. Between-satellite and time-differenced DTDCP test values are calculated to mitigate the effects of the changing datums. A recommended threshold of 2 is applied to determine whether the incoming phase measurement should be treated as new.
(4) Pre-fit residuals consistency check. Ideally, if satellites in the same epoch have no cycle slips and the a priori information is relatively accurate, the calculated misclosures (pre-fit residuals) should be close. This check is as Eq. (10), and the phase pre-fit residuals are divided into two subsets: those from satellite with continuous phase measurements (vector *resi1*) and those from newly recorded phase measurements (vector *resi2*). The mean value and corresponding standard deviation (σ) of *res1* are calculated first. Once the residuals in *resi2* show significant dispersion, inferring that the bridged predicted ambiguity parameter might be incorrect, the corresponding ambiguity and its variance are reset.

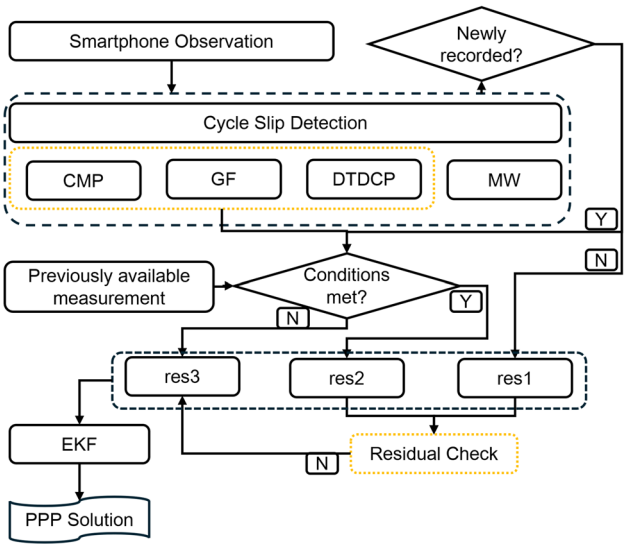

Fig. 3 Simplified flowchart of the proposed algorithm in bridging the phase data gap. CMP, GF, and DTDCP checks are applied to the newly recorded measurements to judge whether to bridge the data gap, residual check is further applied to ensure a reliable bridge

$$\begin{cases} H_0 : mean - k\sigma \le resi_i \le mean + k\sigma \\ H_a : resi_i < mean - k\sigma \,||\, resi_i > mean + k\sigma \end{cases}, \quad resi_i \in resi2 \tag{10}$$

where *mean* is the average of phase pre-fit residuals, k is a threshold factor and is set to 1 in this study.

The simplified flowchart of the proposed algorithms is as Fig. 3. When all the above conditions are met, the phase data gap can be bridged, and therefore, continuous and reliable smartphone positioning results are obtained. The premise of successfully bridging the phase data is the effectiveness of smartphone cycle slip detection methods, and the performance of the applied cycle slip detection-related checks in this study has been investigated in detail by Hu (2024). Therefore, the thresholds used in this study are determined with the consideration of previous analysis of noise levels from different cycle slip detection methods and empirical values.

3 Experiment setup

To validate the proposed phase gap bridging method, smartphone data collected in realistic driving scenarios under suburban environments were processed and analyzed. A total of ten datasets were collected in and around York University, Toronto, Canada, from 2021 to 2022, with data durations of 20–30 min and an interval of 1 s, as summarized in Table 2. The data collection setup is as Fig. 4, in which Xiaomi Mi8

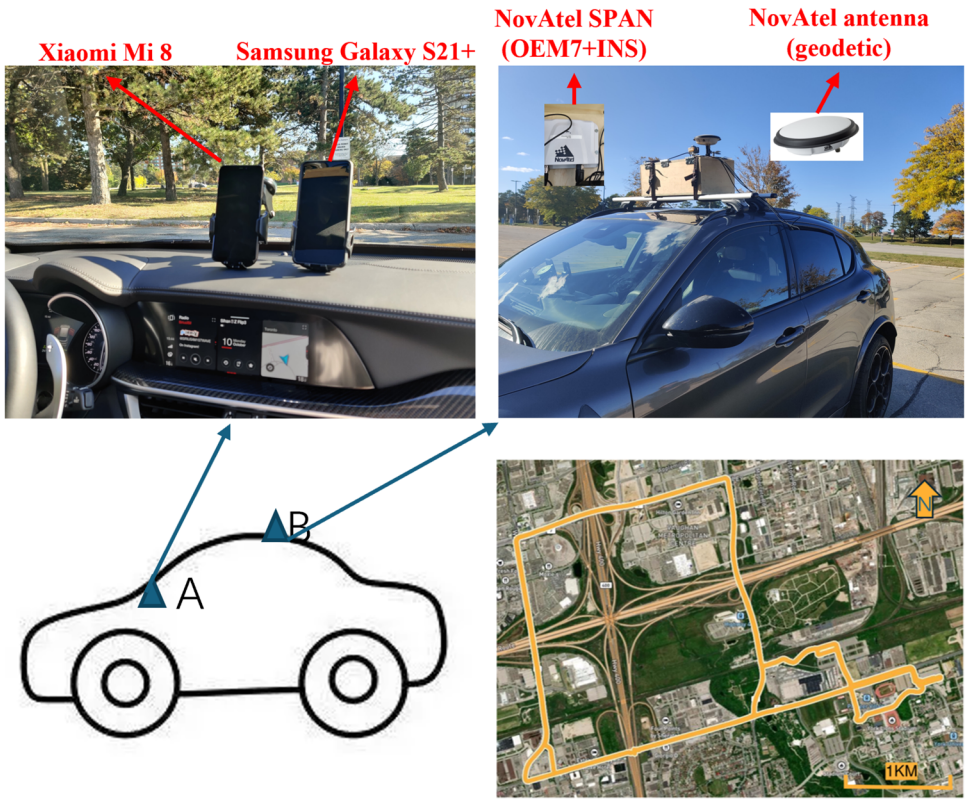

Fig. 4 Smartphone data collection setup and the driving trajectory of data collection areas. Phones were placed on the car dashboard, and reference trajectories were calculated using the higher-grade receiver placed on the car roof. The driving environment contains open-sky, overpass, high-rise buildings and tree blocks

Table 2 Overview of smartphone datasets collected in and around York University

Data index	Smartphone brand	Collection date	Duration (UTC)
1	Mi8	2021–07–30	00:48–01:14
2	Mi8	2021–07–30	01:21–01:46
3	S21 +	2021–08–08	01:52–02:18
4	S21 +	2021–08–20	00:08–00:33
5	Mi8	2021–11–30	02:03–02:29
6	S21 +	2021–11–30	00:54–01:24
7	S21 +	2022–10–09	02:03–02:24
8	Mi8	2022–10–09	01:41–02:01
9	S21 +	2022–11–08	01:54–02:17
10	S21 +	2022–11–08	02:18–02:41

and Samsung Galaxy S21 + smartphones were placed on the car dashboard. The GNSS measurements were recorded using the Geo + + RINEX logger (Wübbena et al. 2018). Additionally, another higher-grade equipment set, NovAtel SPAN (OEM7 + INS), was mounted on the car roof to generate the reference solution. With the lever arm between smartphones and SPAN antenna pre-measured, the commercial software Inertial Explore (IE) was used to produce the PPK/IMU tightly coupled solution, serving as the reference coordinates for smartphones. The data collection trajectory is illustrated at the bottom right of Fig. 4, in which two overpasses (one short and one long) are included.

In PPP processing, the coordinates and receiver clocks are modeled as white noise, i.e., estimated independently between epochs. The ambiguities are estimated as float constants under the conditions that (1) a continuous observed data period without cycle slips is processed, or (2) the missing phase measurements caused by signal loss are bridged using the proposed method. Otherwise, the ambiguity and corresponding variance are reset in the filter. To eliminate the rank deficiency caused by simultaneously estimating ionospheric effects and ambiguities for single-frequency constellations, the Klobuchar model is used as constraint.

4 Results

With the collected datasets, the phase measurement availability is first assessed, followed by a discussion on the efficiency of the proposed satellite-differenced DTDCP method in bridging the phase gaps. Finally, the positioning performance comparison between the proposed measurement bridging method and conventional PPP method is carried out.

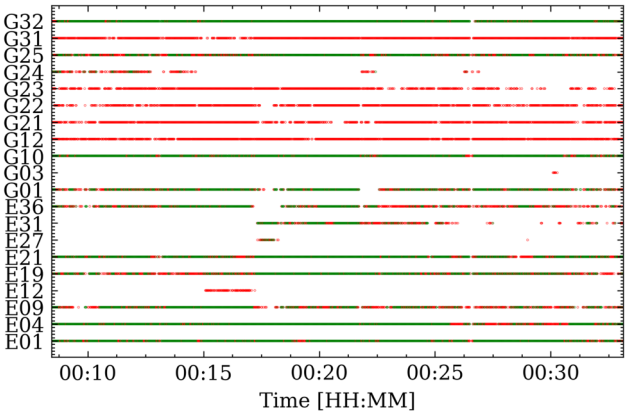

Fig. 5 GPS and Galileo phase measurement availability for dataset collected with a Samsung S21 + phone on August 20, 2021. The red dots represent only single-frequency phase measurements are available, while the green dots denote available dual-frequency measurements

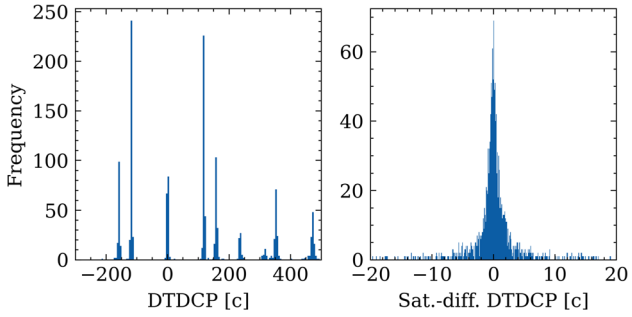

Fig. 6 Distribution of test values of conventional (left) and satellite-differenced (right) DTDCP methods. Conventional method is not applicable in detecting CS, while satellite-differencing successfully eliminates the frequent clock jumps

4.1 Evaluation of phase measurement availability

Unlike measurements collected with geodetic receivers, smartphone GNSS measurements are frequently incomplete. Figure 5 depicts the phase measurement availability of GPS and Galileo satellites collected by a Samsung S21 + phone on August 20, 2021. The red and green dots denote single- and dual-frequency phase measurements, respectively. It is evident that dual-frequency measurements are only available for a subset of GPS satellites. All the measurements were lost at around 00:26 because the car passed under a long overpass, which obstructed the GNSS signals. For some satellites, the measurement integrities are relatively high, e.g., E01, G10, and G32. However, for others, the phase measurements are frequently missing on both L1 and L5 frequencies, which will lead to frequent resets of ambiguity parameters, negatively affecting the positioning accuracy. The measurement availability assessment further highlights the importance of the proposed method for bridging the phase gaps. For shorter data gaps, such as those lasting only a few seconds, the ambiguities before and after the gap may remain unchanged and can potentially be bridged using cycle slip detection methods.

4.2 Efficiency of satellite-differenced DTDCP measurements

The distribution of the differences between Doppler and TDCP measurements before and after satellite-differencing for the to-be-bridged phase candidates is analyzed. Figure 6 illustrates the distributions of the test values calculated with conventional (left subplot, based on Eq. (6)) and modified (right subplot, based on Eq. (9)) DTDCP cycle slip detection methods. Eight significant clusters are noticed in the left subplot, indicating that when setting a fixed empirical threshold to bridge the phase gaps, most trials are rejected. These clusters are caused by frequent phase clock jumps as illustrated in Fig. 1. The clocks do not regularly jump, i.e., the jumps do not happen in a periodical manner, and the jump amplitudes are different and are hard to predict when the time intervals for different measurements are various. By performing satellite-differenced DTDCP measurements, the effect of the inconsistent phase jumps among epochs can be mitigated, as demonstrated in the right subplot. The reason is that the jumps are consistent for measurements on the same frequency and within the same constellation (Hu et al. 2024). Hence, the improved satellite-differenced DTDCP measurement can be used in bridging the phase gaps by selecting an appropriate threshold. The test value distributions confirm the efficiency of the proposed modified DTDCP method.

4.3 Positioning performance validation

This section starts with the detailed positioning results analysis for two specific datasets collected with Mi8 and S21 + phones, respectively, to provide insight into how the proposed method performs in the time series of positioning errors. Moreover, the positioning statistics for different smartphone models are calculated, to show smartphone model-specific improvements. Finally, positioning performance comparisons for all datasets are conducted.

When all the proposed conditions for bridging the phase gaps (i.e., CMP, GF, satellite-differenced DTDCP, and phase pre-fit residual checks) are satisfied, the corresponding ambiguities and their variance will not be reset, and the previously available information is utilized as predictions in EKF. Ten datasets were processed, and the horizontal positioning performance was analyzed by comparing the proposed bridging method with conventional PPP results. Key performance metrics, including the 68th and 95th percentile positioning errors (abbreviated as per.68 and per.95), corresponding root-mean-square (rms) values (abbreviated as RMS.68 and RMS.95), and the percentages of positioning errors within 1.5 m and 1 m were calculated. The percentiles are used to

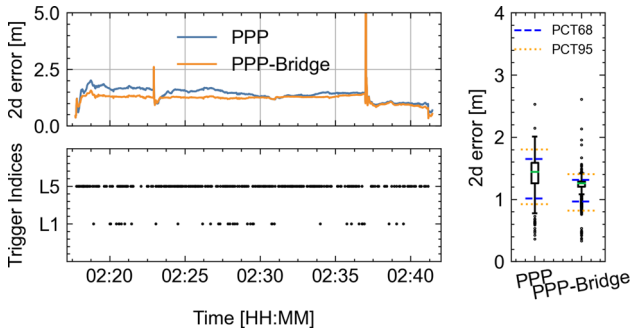

Fig. 7 Time series of horizontal positioning errors and bridge trigger indices for datasets collected on November 8, 2022 with a Samsung S21 + phone (dataset #10). Box plot shows the horizontal error distribution of PPP and PPP-Bridge solutions

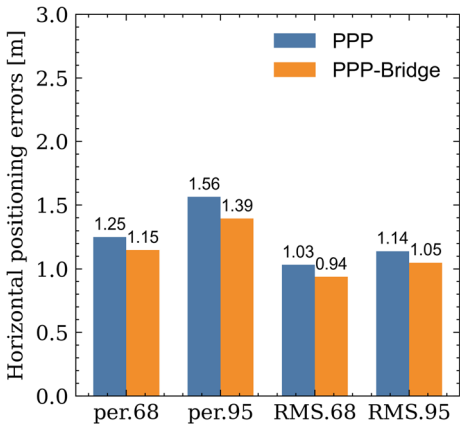

Fig. 8 Horizontal positioning performance comparison between PPP and PPP-Bridge solutions for all Samsung S21 + datasets. The 68th and 95th percentiles, as well as the corresponding rms values are calculated and compared

indicate the large positioning errors, while the corresponding rms values are used to reflect the solution stability.

4.4 Positioning performance analysis for different smartphone models

First of all, specific horizontal positioning error time series for a Xiaomi Mi8 (dataset #2) and a Samsung S21 + (dataset #10) phone are presented for detailed analysis, as shown in Figs. 7 and 9. In these figures, the trigger indices for phase gap bridging on L1 and L5 are also illustrated. It should be noticed that there are two spikes, which are caused by the signal loss when the vehicle was passing the overpasses. The black dots indicate instances where at least one phase measurement has been bridged. The proposed method is frequently triggered on L5 and performs effectively in providing continuous and stable positioning solutions. For the results in Fig. 7, the bridged solution maintains the same accuracy level after the first small spike (at ~ 02:23). Notably, 99.1% of the positioning errors are within 1.5 m, while it is only 65.1% with conventional method. Furthermore, the 68th percentile positioning errors are reduced from 1.53 m to 1.28 m, while those of 95th percentile are reduced from 1.75 m to 1.37 m, achieving accuracy improvements of 2–4 dm.

The positioning performance comparison for all Samsung S21 + datasets is conducted and illustrated in Fig. 8. With 5784 available epochs, the percentage of horizontal positioning errors within one meter is improved from 27.0% to 47.0%, representing an enhancement of 20%. For all the calculated horizontal positioning errors, the proposed method outperforms conventional PPP results, with the 68th percentile errors reduced by 0.1 m and 95th percentile errors reduced from 1.56 m to 1.39 m, demonstrating a higher ability in providing high-accuracy positioning results.

In terms of the results for one of the Xiaomi Mi8 phones, as shown in Fig. 9, the proposed method consistently outperforms the conventional method across all the epochs. The

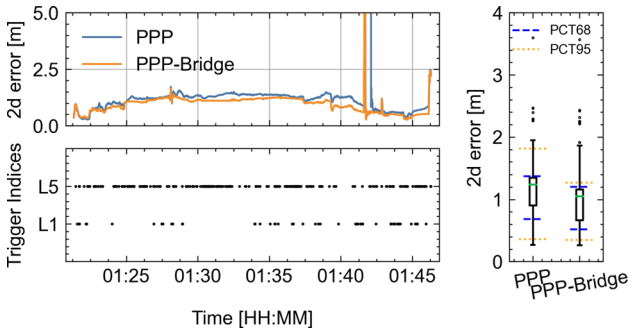

Fig. 9 Time series of horizontal positioning errors and bridge trigger indices for datasets collected on July 30, 2021 with a Xiaomi Mi8 phone (dataset #2). Box plot shows the horizontal error distribution of PPP and PPP-Bridge solutions

most significant improvement is noticed after the spike at ~ 01:42. After the overpass, the conventional method has large positioning errors for the subsequent epochs, whereas the proposed method successfully utilized the information before the spike, obtaining a high-accuracy solution right after the spike. The 95th percentile positioning errors are reduced from 1.45 m to 1.25 m, and those of the 68th percentile are reduced from 1.31 m to 1.13 m, representing improvements of 13.8% and 13.7%, respectively.

Similarly, the positioning results for all Xiaomi Mi8 datasets are depicted in Fig. 10. There are 8853 epochs in total, and the percentages of horizontal errors within 1 and 1.5 m are improved by 0.5% and 7.4%, respectively. The most obvious improvement is the 95th percentile positioning errors, of which the positioning errors are reduced from 1.71 m to 1.53 m.

Table 3 Horizontal positioning statistics for processed 10 datasets (units: m)

	Per68	RMS.68	Per95	RMS.95	Within 1.0 m	Within 1.5 m	Epochs
PPP	1.32	1.07	1.65	1.19	31.1%	76.1%	14,637
PPP-Bridge-noResidualCheck	1.32	1.05	1.57	1.18	32.3%	74.1%	14,637
PPP-Bridge	1.26	1.01	1.47	1.13	39.3%	80.4%	14,637

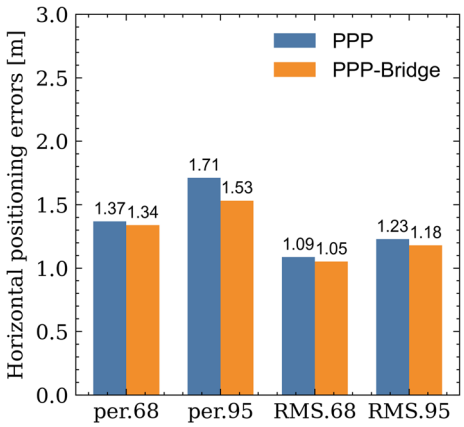

Fig. 10 Horizontal positioning performance comparison between PPP and PPP-Bridge solutions for all Xiaomi Mi8 datasets. The 68th and 95th percentiles, as well as the corresponding rms values are calculated and compared

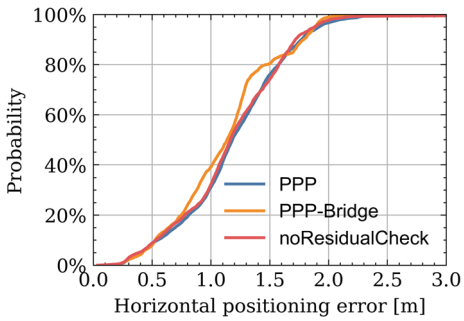

Fig. 11 CDF of horizontal positioning errors for processed 10 datasets with PPP, PPP-Bridge, and noResidualCheck schemes

4.5 Positioning performance analysis for all datasets

The statistics for all ten datasets are calculated as well, as summarized in Table 3, and the corresponding cumulative distribution function (CDF) is plotted in Fig. 11. As there is a risk in wrongly bridging the phase measurements, the residual check (Eq. (10)) is performed. To demonstrate the effectiveness and practical relevance of this condition, a scheme that the residual check is not performed is designed, namely PPP-Bridge-noResidualCheck. With a total of 14,637 available epochs, the proposed phase gap bridge method outperforms the conventional PPP method across all listed metrics. The positioning errors within 1.5 m

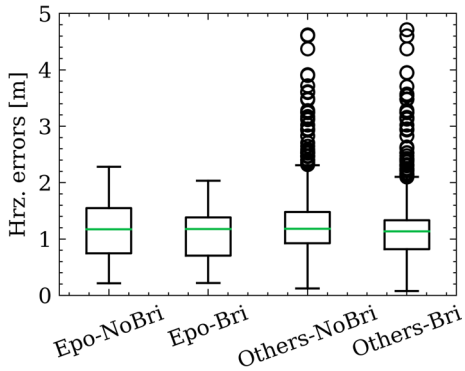

Fig. 12 Boxplots of horizontal positioning errors for epochs that bridge is applied (Epo-Bri) and not applied (Epo-NoBri), as well as the errors for other indirectly affected epochs (Others-NoBri and Others-Bri)

and 1 m are improved by 4.3% and 8.2%, respectively, demonstrating a stronger capability of providing lane-level navigation and sub-meter positioning performance with the proposed method. The larger positioning errors, represented by the 95th percentile positioning errors, are reduced from 1.65 m to 1.47 m, achieving an improvement of ~ 2 dm. Almost all the positioning errors with the proposed method fall within 2 m, whereas a few errors exceed 2 m for the conventional method. When the residual check is not applied, the positioning performance can be slightly improved compared to conventional PPP results. In contrast, when applying the residual check, the performance enhancement is significant, inferring that with this check, the ambiguities are bridged reliably. The positioning results analysis indicates that the proposed method not only mitigates large positioning errors but also maintains a stable positioning solution.

To directly assess the effectiveness of the proposed method, positioning errors specifically at the epochs when bridging is applied are evaluated. Positioning errors of four categories are calculated: epochs that bridges are conducted on L1 or L5 (Epo-Bri), corresponding epochs of conventional PPP (Epo-NoBri), Other epochs that bridges are not performed for PPP-Bridge solution (Others-Bri), and conventional PPP solution (Others-NoBri). The boxplot is shown as Fig. 12, and the phase gap bridge not only improves the positioning accuracy for the bridged epochs, but also for those without directly bridging. The reason is that EKF is applied in data processing, and the previous state vector will

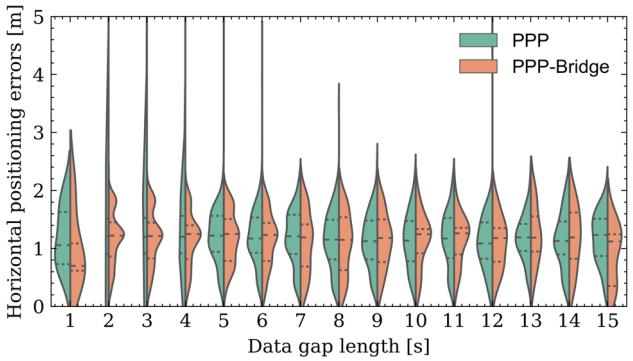

Fig. 13 Violine plot of horizontal positioning error comparison with different data gap lengths between conventional PPP solutions and the proposed methods

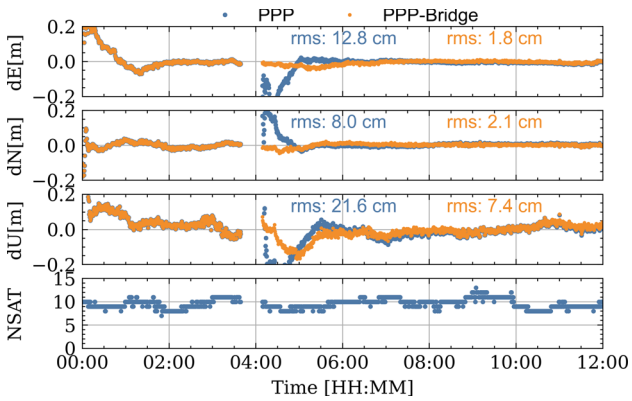

Fig. 14 Positioning performance comparison between PPP and PPP-Bridge solutions with geodetic receiver experiment for station KMNM on DOY 122, 2024. The GNSS data were not recorded during 03:30–04:00

be used as a prediction for the subsequent epochs. For epochs that bridges are directly applied, the 25th quantile (Q1) positioning error is reduced from 0.75 m to 0.70 m, while those for other epochs are indirectly improved from 0.93 m to 0.82 m. Moreover, the upper line of the box plot, i.e., 75th quantile (Q3), indicates that large positioning errors are reduced through the proposed method, representing improved accuracy of 0.17 m and 0.15 m for epochs where bridges are directly applied and others, respectively.

As past observations are used as reference when bridging the gaps, the covariance of prediction might not be accurate over long durations. Therefore, a detailed assessment of the performance of the bridging mechanism for various gap lengths is conducted, and the results are provided in Fig. 13. Most data gaps are within several seconds, e.g., 2–10 s, and hence, data gap lengths varying from 1 to 15 s are displayed. The median values, as well as the Q1 and Q3 statistics, are labeled in the plot. It is clear that the PPP-Bridge solutions outperform conventional PPP performance for almost all data gap lengths. When the data gap is less than 7 s, the large errors are significantly reduced with the proposed method, and labeled statistics are more precise than conventional PPP solutions. Slight accuracy degradation for Q3 is noticed when the gaps are 13 and 14 s, which is possibly caused by the inaccurate predicted ambiguities. Furthermore, when the gap is 15 s, significant improvement can still be realized.

4.6 Results and discussion on potential applications in geodetic receivers

To validate the potential applications of the proposed algorithm in fields except for smartphones, an experiment with geodetic-grade receiver is carried out. Data from station KMNM on day of year (DOY) 122 in 2024 are processed in PPP-simulated kinematic mode. Noting that all the measurements were not recorded during 03:30–04:00, and the conventional solution reconverges when the measurements came back. The bridge procedure was only triggered once when the measurements were available again. Therefore, when concentrating on the bridged epoch, the bridged solution is significantly better than the conventional PPP results. The positioning differences observed between 05:00 and 06:00 are partly due to the convergence process and are less related to the proposed method. The positioning root-mean-square values for one hour after the bridge applied are calculated. When bridging the phase gaps, the average positioning accuracy can be improved from 12.8, 8.0, and 21.6 cm to 1.8, 2.1, and 7.4 cm in the east, north, and up directions, respectively, compared to conventional PPP solutions. Despite such a long signal outage occurs, by carefully applying the data bridge conditions, the proposed algorithm successfully maintains high-accuracy performance, demonstrating that the proposed method not only performs well in smartphone data processing, but also shows great potential in improving positioning performance of high-grade receivers (Fig. 14).

5 Conclusion

Frequent missing measurements are thorny in smartphone GNSS data processing, as the missing phase measurements lead to frequent ambiguity and variance resets in the filter, which consequently degrades the positioning performance in traditional algorithm. To address this issue, this study proposes bridging the phase data gaps from the perspective of cycle slip detection. CMP, GF, modified DTDCP, and phase pre-fit residuals are used as indicators for the transition of ambiguity and variance. Ten smartphone datasets collected in realistic driving environments were processed. Measurement availability assessment, validation of the efficiency of the improved DTDCP method, as well as the positioning

performance comparison were conducted to validate the proposed method.

The assessment of phase measurement availability reveals that phase measurements from most satellites are frequently lost, resulting in varying data gaps. Once the gaps without cycle slips are correctly identified, i.e., the data gaps can be bridged, it is expected to enhance the positioning solution. Additionally, the conventional DTDCP is inapplicable in data bridging because of the irregular phase jumps in smartphones. Therefore, an improved DTDCP method is proposed by forming satellite-differenced DTDCP, in which the jump datums can be successfully eliminated. Test values derived from the improved DTDCP method follow a zero-mean generalized normal distribution. With an appropriately selected threshold, phase data can be successfully bridged.

Two specific positioning examples show significant improvements with the proposed method compared to conventional PPP results. The percentage of positioning errors within 1.5 m increases from 65.1% to 99.1% for a Samsung S21 + phone (dataset #10), nearly achieving lane-level navigation throughout the entire time period. In another Xiaomi Mi8 dataset (#2), the 68th and 95th percentile positioning errors are improved by ~ 2 dm. The overall statistics with 10 datasets further demonstrate the correctness and efficiency of the proposed method, in which the positioning errors within 1.5 m and 1 m are improved by 4.3% and 8.2%, respectively.

In conclusion, the proposed method enables more stable and accurate positioning performance. By correctly bridging the phase gaps, the possibility of the smartphones used as lane-level navigation sensors is obviously improved. Moreover, potential applications that require sub-meter-level positioning accuracy could also be realized with smartphones. Moreover, the measurements from low Earth orbit (LEO) satellites and observations from mass-market low-cost equipment might also suffer from phase loss, but not that frequently. The proposed method is anticipated to have better performance in these measurements, as when more dual-frequency measurements are available, the gaps can be bridged with higher confidence level than smartphones.

Acknowledgements This research was supported by the National Natural Science Foundation of China (Grant No. 42374026, 42274034, and 42104015), the Hong Kong Polytechnic University (No. A0048555), the Research Funds for the Interdisciplinary Projects, CHU (Grant No. 300104240914), the Fundamental Research Funds for the Central Universities, CHD (Grant No. 300102263401), Guangdong Basic and Applied Basic Research Foundation (Grant No. 2023A1515030184), Guangzhou Science and Technology Plan Project (Grant No. 2025A04J5190), and Natural Science Foundation of Hubei Province (No. 2025AFB652).

Author contributions Hu J did idea proposing, software design, manuscript writing and revision; Chen W developed funding acquisition, idea discussion, and supervision; Li P did code implementation, manuscript writing and reviewing; Mi X did idea discussion and preliminary results analysis; Zheng K and Tang L did data analysis; Liu W did idea proposing and optimization, manuscript revision; Yuan J did initial validation of smartphone cycle slip detection and figure generation; Bisnath S did software design, manuscript editing, and idea development.

Data availability The GNSS final precise satellite orbit and clock products provided by GFZ are available at ftp://ftp.gfz-potsdam.de/GNSS/products/mgex/. The smartphone observation data are available upon reasonable requests.

Declaration

Conflict of interest The authors declare no competing interests.

References

Bisnath S, Aggrey J (2024) Current limitations and prospects for smartphone GNSS precise positioning. In: Proceedings of the 2024 International Technical Meeting of The Institute of Navigation, California, USA, 1–24. https://doi.org/10.33012/2024.19560

Blewitt G (1990) An automatic editing algorithm for GPS data. Geophys Res Lett 17:199–202

Everett T, Taylor T, Lee DK, Akos DM (2022) Optimizing the use of RTKLIB for smartphone-based GNSS measurements. Sensors 22(10):3825

Fu G, Khider M, Van Diggelen F (2020) Android raw GNSS measurement datasets for precise positioning. Proc ION GNSS 2020, Institute of Navigation, 21–25, 1925–1937

Hu J, Yi D, Bisnath S (2023) A comprehensive analysis of smartphone GNSS range errors in realistic environments. Sensors 23(3):1631

Hu J, Li P, Bisnath S (2024) Enhancing smartphone precise point positioning to sub-meter accuracy in suburban environments: a new stochastic model and outlier diagnosis. GPS Solut 28:112

Hu J (2024) Why some cycle slip detection methods do not work for smartphones: investigation, explanation and solutions. In: Proceedings of the 37th international technical meeting of the satellite division of the institute of navigation (ION GNSS+ 2024), 16–20, pp 2541–2554

Huang G, Du S, Wang D (2023) GNSS techniques for real-time monitoring of landslides: a review. Satell Navig 4:5. https://doi.org/10.1186/s43020-023-00095-5

Jiang Y, Gao Y, Ding W, Liu F, Gao Y (2023) An improved ambiguity resolution algorithm for smartphone RTK positioning. Sensors 23(11):5292. https://doi.org/10.3390/s23115292

Kouba J (2009) A guide to using International GNSS Service (IGS) products. https://igscb.jpl.nasa.gov/igscb/resource/pubs/UsingIGSProductsVer21.pdf

Langley R, Teunissen P, Montenbruck O (2017) Ionosphere Monitoring. In: Teunissen PJG, Montenbruck O (eds) Springer handbook of global navigation satellite systems. Springer International Publishing, 3–24

Laurichesse D, Rouch C, Marmet F, Pascaud M (2017) Smartphone applications for precise point positioning. *Proc. ION GNSS 2017*, Institute of Navigation, Portland, Oregon, September 25–29, 171–187

Li Z, Wang L, Wang N, Li R, Liu A (2022a) Real-time GNSS precise point positioning with smartphones for vehicle navigation. Satellite Navigation 3:19. https://doi.org/10.1186/s43020-022-00079-x

Li X, Wang H, Li X, Li L, Lv H, Shen Z, Xia C, Gou H (2022b) PPP rapid ambiguity resolution using Android GNSS raw measurements with a low-cost helical antenna. J Geod 96:65

Liu W, Shi X, Zhu F, Tao X (2019) Wang f (2019) Quality analysis of multi-GNSS raw observations and a velocity-aided positioning approach based on smartphones. Adv Space Res 63:2358–2377

Malkos S (2016) User location takes center stage in new Android OS: Google to provide raw GNSS measurements. GPS World 27:36

Miao W, Li B, Gao Y (2022) The superiority of multi-GNSS L5/E5a/B2a frequency signals in smartphones: stochastic modeling, ambiguity resolution, and RTK positioning. IEEE Internet Things J 10(8):7315–7326. https://doi.org/10.1109/JIOT.2022.3228769

Paziewski J, Sieradzki R, Baryla R (2019) Signal characterization and assessment of code GNSS positioning with low-power consumption smartphones. GPS Solut 23:98

Paziewski J, Pugliano G, Robustelli U (2020) Performance assessment of GNSS single point positioning with recent smartphones. In: IMEKO TC-19 international workshop on metrology for the sea. Naples, Italy

Realini E, Caldera S, Pertusini L, Sampietro D (2017) Precise GNSS positioning using smart devices. Sensors 17:2434

Robustelli U, Baiocchi V, Pugliano G (2019) Assessment of dual frequency GNSS observations from a Xiaomi Mi 8 Android smartphone and positioning performance analysis. Electronics 8(1):91

Shu B, Lei T, Li P, Wang L, Huang G, Zhang S, Zhang Q (2025) Calibration of inconsistent receiver-dependent pseudorange bias and its impact on wide-lane ambiguity fixing. GPS Solut 29:64. https://doi.org/10.1007/s10291-025-01825-9

Sikirica N, Malić E, Rumora I, Filjar R (2017) Exploitation of Google GNSS measurement API for risk assessment of GNSS applications. In: 2017 25th telecommunication forum (TELFOR) (pp 1–3). IEEE

Tao X, Liu W, Wang Y, Li Y, Zhu F, Zhang X (2023) Smartphone RTK positioning with multi-frequency and multi-constellation raw observations: GPS L1/L5, Galileo E1/E5a, BDS B1I/B1C/B2a. J Geodesy 97:43. https://doi.org/10.1007/s00190-023-01731-3

Wang L, Li Z, Wang N, Wang Z (2021) Real-time GNSS precise point positioning for low-cost smart devices. GPS Solut 25:69. https://doi.org/10.1007/s10291-021-01106-1

Wang J, Shi C, Zheng F, Yang C, Liu X, Liu S, Xia M et al (2024) Multi-frequency smartphone positioning performance evaluation: insights into A-GNSS PPP-B2b services and beyond. Satell Navig 5:25. https://doi.org/10.1186/s43020-024-00146-5

Wübbena T, Darugna F, Ito A, Wübbena J (2018) Geo++'s Experiments on android GNSS raw data. In: GNSS raw measurements taskforce workshop, GSA Headquarters, 2018, Prague

Yi D, Hu J, Bisnath S (2024) Improving PPP smartphone processing with adaptive quality control method in obstructed environments when carrier-phase measurements are missing. GPS Solut 28:56. https://doi.org/10.1007/s10291-023-01596-1

Zangenehnejad F, Jiang Y, Gao Y (2022) Improving smartphone PPP and RTK performance using time-differenced carrier phase observations. In: Proceedings of the 35th international technical meeting of the satellite division of the institute of navigation (ION GNSS+ 2022), 19–23, 2287–2300

Zangenehnejad F, Gao Y (2021) GNSS smartphones positioning: advances, challenges, opportunities, and future perspectives. Satellite Navig 2(1):24. https://doi.org/10.1186/s43020-021-00054-y

Zhang Y, Jiang Y, Gao Y, Guo S, Gao Y (2024) An improved wide-lane ambiguity resolution method for kinematic smartphone positioning. J Navig 77:1–17. https://doi.org/10.1017/S0373463324000158